Model predictive control based real-time scheduling for balancing multiple uncertainties in integrated energy system with power-to-x

Turk, Ana; Wu, Qiuwei; Zhang, Menglin

Published in:
International Journal of Electrical Power & Energy Systems

Link to article, DOI:
10.1016/j.ijepes.2021.107015

Publication date:
2021

Document Version
Peer reviewed version

Model predictive control based real-time scheduling for balancing multiple uncertainties in integrated energy system with power-to-x

Ana Turk[a], Qiuwei Wu[a,*], Menglin Zhang[a,*]

a Center for Electric Power and Energy (CEE), Department of Electrical Engineering, Technical University of Denmark (DTU), Kgs. Lyngby 2800, Denmark

Abstract

Integration of the electric power system, natural gas system, and district heating system can reduce the operational cost and improve the utilization of renewable energy sources. The day-ahead schedule for the optimal operation of the integrated energy system may not be economically optimal in real-time due to the prediction errors of multiple uncertainty sources. To balance the real-time prediction errors economically, this paper proposes a model predictive control (MPC) based real-time scheduling strategy to optimize the real-time operation of the integrated energy system, which makes real-time operational decisions based on the measured state of the system and future information of uncertainties. In the MPC based real-time scheduling, the penalty for the deviation between the day-ahead and real-time schedules is considered to minimize the regulation cost. In addition, multiple uncertainty sources are taken into account. An online learning method is utilized in MPC to predict the future information of these uncertainties. Besides, the power-to-x technology and thermal energy and gas storage devices are considered to improve the capability of the system to balance these uncertainties. The simulation results show that the MPC based real-time scheduling outperforms the traditional real-time scheduling on economic efficiency and wind power utilization.

Keywords:

Integrated energy system, model predictive control, online learning, real-time scheduling, prediction horizon, wind power uncertainty

Nomenclature

Symbol	Description	Unit
	Sets	
$n,m \in \Lambda^{EPS/DHS/NGS}$	Sets of nodes in the EPS/DHS/NGS	
$j \in \Omega^{CHP}$	Set of CHP	
$f \in \Omega^{WF}$	Set of wind farms	
$e \in \Omega^{ED}$	Set of electric demand	
$h \in \Omega^{HS}$	Set of thermal energy storage	
$l \in \Omega^{HL}$	Set of thermal demand	
$p \in \Omega^{P2G}$	Set of P2G	
$g \in \Omega^{GS}$	Set of gas source	
$s \in \Omega^{ST}$	Set of gas storage	
$g \in \Omega^{GC}$	Set of gas compressor	
$d \in \Omega^{GD}$	Set of gas demand	
	Constants	
$\lambda_{mn,t}$	Thermal conductivity of pipeline	W/mK
λ_g^{GC}	Operational energy consumption coefficient of GC	
$\eta_g^{GC}, \eta_p^{P2G}$	Compression efficiency of GC, energy conversion efficiency of at the P2G	
η_j^e, η_j^h	Generating electrical and thermal efficiency of CHP	
τ^a	Ambient temperature	°C
B_{nm}	Susceptance of transmission line	p.u.
C	Water specific heat capacity	J/kgK
c_k, CR	Natural gas specific heat ratio, compression ratio	

*Corresponding author: Q. Wu (e-mail: qw@elektro.dtu.dk), M. Zhang (e-mail: menzh@elektro.dtu.dk).

$C, C^{penalty}$	Marginal cost of units and penalty for deviating from DA	\$/MWh
C_e^{VOLL}, C_f^{spill}	Value of lost load, wind spillage cost	\$/MWh
$D_{d,t}^{GD}, D_{e,t}^{ED}, H_{l,t}^{HL}$	Demand: gas, electric, thermal	MW
E^{GC}, K^{GC}	GC parasitic efficiency, GC constant	
L_{mn}	Length of pipeline	m
RLD_j^{CHP}, RLU_j^{CHP}	Downward and upward ramping rate limit of CHP	MW/h
T_s, Z_a	GC suction temperature, average compressibility factor	°R, -
$W_{f,t}^{max}, W_{f,t}^{RT}, W_{f,t}^{DA}$	Wind output power: nominal, measured, forecasted	MW
Z_{nm}	Pipeline resistance coefficient	$kPa^2/(MW)^2$
	Variables	
$\delta_{n,t}$	Phase angle of bus *n*	rad
$\tau_{mn,t}^{in}$	Temperature of inlet to node n of pipe m-n	°C
$\tau_{mn,t}^{out}$	Temperature of outlet of node m of pipe m-n	°C
$D_{j,t}^{CHP}, D_{g,t}^{GC}$	Gas consumption of : CHP and gas compressor	MW
$D_{e,t}^{ED,shed}, D_{p,t}^{P2G}$	Load shedding, power demand of the P2G	MW
$H_{j,t}^{CHP}$	Heat supply from CHP	MW
$H_{h,t}^{HS,in}, H_{h,t}^{HS,out}$	Heat output: from the TES to heat network, from the heat network to TES	MW
$HS_{h,t}$	Heat stocks in TES	MWh
$m_{mn,t}$	Water flow rate in pipe	kg/s
$p_{n,t}^2$	Gas pressure at node n	MPa^2
$P_{j,t}^{CHP}$	Power supply from CHP	MW
$Q_{g,t}^{GS}, Q_{p,t}^{P2G}$	Gas supply from: gas source, P2G	MW
$Q_{s,t}^{ST,in/out}$	Gas input/output of storage	MW
$S_{mn,t}, S_{g,t}^{GC}$	Gas flow rate in: pipeline, through gas compressor	MW
$ST_{s,t}$	Gas stocks in storage	MWh
$W_{f,t}^{spill}$	Spillage of wind unit *f*	MW
$x_{s,t}^{ST,in}, x_{s,t}^{ST,out}$	Binary variables	
$x_{h,t}^{HS,in}, x_{h,t}^{HS,out}$	Binary variables	

1. Introduction

The installed capacity of renewable energy sources (RES) has been increasing at a high rate where wind power is the major RES [1]. According to the Paris Agreement, the limit on the increase of the global average temperature below two degrees is pushing towards the decrease of CO_2 emissions and an increase of RES [2]. As conventional generators are phased out and more fluctuating RES based units are integrated, the system faces operation and control challenges. In Denmark, around 64% of the electricity supply is based on RES, whereas more than half is from solar and wind power [3]. To reduce CO_2 emissions and maintain the secure operation of the energy system with a high share of RES, the integration of different energy sectors is essential to provide sufficient flexibility. With the transition towards a 100% renewable based energy system, the power to x (P2X) including the power to gas (P2G) will play a major role in balancing the energy systems in Denmark [4]. With interactions between different energy sectors through P2X, it is possible to shift consumption and increase the flexibility of the system [5].

The integration of different energy sectors has been extensively investigated. Refs. [6], [7] and [8] provide an overview of the modelling and integration of the natural gas system (NGS) and electric power system (EPS). Ref. [6] increases the flexibility and reduces the total energy losses by the integration of the NGS and EPS with the P2G unit. Ref. [7]

formulates the linear model of the integrated system and considers the linepack to reduce operational costs and improve system flexibility. Ref. [8] optimally adjusts the NGS price to reduce the expected system cost and considers the temporal correlation between day-ahead (DA) and real-time (RT) markets. The efficiency of accommodating RES in the EPS increases by using the stochastic methodology. Refs. [9] and [10] develop models for the integrated EPS and district heating system (DHS). Ref. [9] validates higher flexibility and accommodation of wind power by integrating the EPS and DHS compared to the separate optimization of the EPS and DHS. Ref. [10] considers the coordination and joint operation of the EPS and DHS, which outperforms the optimal dispatch based on the decomposed method in the iteration number. Ref. [11] integrates the EPS, DHS and NGS to achieve higher feasibility and efficiency of the integrated energy systems (IES) by utilizing the two-stage stochastic programming approach.

There are multiple uncertainty sources in the IES, such as the RES, electricity demand, heat load, and gas demand, which may lead to the imbalance between production and consumption in the RT stage. Among these uncertainty sources, the RES is the main reason for system imbalance, which usually has larger prediction errors compared to the rest of uncertainties [12]. Due to the prediction error of the uncertainty sources, the DA schedule for the optimal operation of the IES may not be economically optimal in the RT stage. In order to balance the uncertainties in an economic way, the RT scheduling of the IES is essential. The traditional RT scheduling of the IES is a single-period optimization, which only considers the measured values of each uncertainty source in the current step. Without accounting for the future information of the uncertainties, the traditional RT scheduling cannot obtain the global optimum for the entire scheduling horizon. A promising solution to cope with this is the model predictive control (MPC) strategy. The MPC strategy can deal with the uncertainties of the RES in a forward-looking way when optimizing the hourly schedule. It considers the response of current decisions to future uncertainties [13]. In summary, the MPC strategy optimizes the schedule for the long run, bringing a more economical decision than the traditional RT scheduling.

In [13], the MPC is utilized to minimize the operational costs of a microgrid, considering the uncertainty of the electric load, prices and wind power. The forecast errors follow a probability distribution with zero mean and a known standard deviation. Ref. [14] proposes an MPC strategy to minimize the RT cost of a nonlinear model of the integrated EPS and NGS with energy storage. Refs. [15] and [16] investigate the MPC based adaptive and corrective scheduling in the microgrids, which minimize the operational cost and penalize the deviation from the DA schedule to evaluate the available flexibility in the system. In Ref. [15], the flexibility provided by multi-energy system units is explored by intraday adjustments of operational points of the flexible units. Such rescheduling based on MPC in the intraday market shows the possibility of balancing the uncertainties of the RES and electricity demand. Ref. [16] explores various configurations of multi-energy microgrids. The combination of centralized and distributed MPC based scheduling provides the most efficient solution in terms of high flexibility, reduced total system costs, and wind curtailment. In the MPC based optimization, the prediction horizon is a key parameter that may influence the forecast accuracy, computational burden, and decision results. Refs. [13, 14, 17] select the prediction horizons based on the standard deviation of the forecast error which follow a normal distribution. In Refs. [15] and [17], the prediction horizons are set as 48 and 24 time steps, respectively, and the standard deviation increases linearly with the time from the current time step. At the end of the prediction horizon, the maximum forecasting error is considered. Overall, when selecting the prediction horizon, the computational burden, storage capacities, and forecast errors must be considered [14]. Moreover, a long prediction horizon results in high computation. On the contrary, a short prediction horizon has a lower computational burden. However, the short prediction horizon may result in a local optimization that fails to capture the optimal solution [18]. Furthermore, the stochastic MPC has been applied to consider the uncertainty and variability of RES and load in [18]-[22]. In [18], the stochastic MPC minimizes the system operational costs and handles the charging pattern of the electric vehicles and variability of RES. However, the uncertainty of demand variability is not considered. Furthermore, the stochastic MPC is applied for reconfiguration of the electric distribution grid while taking into account the variability of RES [19]. Such an approach results in increased robustness concerning the prediction errors and outperforms the simple stochastic approach. The total cost is higher with the simple stochastic approach compared to the stochastic MPC based approach. In [21], the stochastic MPC has been applied to the scheduling of appliances in a smart home. The optimal control of the energy storage systems based on the stochastic MPC has been performed in [22] which reduces the total system costs and energy losses. In summary, the MPC has numerous applications. However, it has not been applied to the IES. Therefore, this work focuses on the MPC strategy

for the RT scheduling of an IES and considers several uncertainties. The multiple uncertainty sources include the electricity demand, heat load, gas demand, and wind power output.

In summary, the previous work based on MPC is mainly focused on the operation of the microgrid. The RT operation of the integrated EPS, DHS and NGS based on MPC is very limited. This paper develops an MPC based RT scheduling strategy for the IES to achieve higher flexibility and economic efficiency while accounting for multiple uncertainty sources. The main contributions of this work are summarized as follows:

- This paper proposes a real-time scheduling scheme for the IES based on MPC aiming to reduce operational cost, improve utilization of RES and increase flexibility by integrating the online learning (OL) method into MPC. MPC explores the possibility of the energy storages and P2G to provide balancing energy by penalizing the deviation from the DA schedule;
- Multiple uncertainty sources are taken into account for the real-time schedule of the IES, including the electricity demand, heat load, gas demand, and wind power outputs. The OL method combined with MPC is used to provide time-efficient and accurate forecasts one step ahead for the MPC to reduce future forecast error;
- The prediction horizon length of the MPC is properly selected according to the computational efficiency, economic efficiency, wind power utilization, and storage capacity.

The rest of the paper is organized as follows. Section 2 gives an overview of the traditional RT scheduling and presents the strategy of MPC based RT scheduling for the IES. Section 3 formulates the MPC based RT scheduling model of the IES and summarizes its solution process. Section 4 gives the simulation results, followed by the conclusions.

2. Framework of MPC based RT scheduling and MPC strategy

2.1 Traditional RT scheduling

The daily scheduling is performed in three markets, i.e. DA market, intraday market and RT market. The RT market is followed by the DA and intraday market. The additional explanations are not given to DA and intraday market, and for simplicity, the intraday market is neglected. The following elaborations are based on the RT balancing used in the Nordic market [23, 24, 25, 12]. The RT market, often called the balancing market, maintains the balance between the production and consumption during the operational hour. The traditional Nordic RT electricity market is a single-period optimization and it is divided into the regulating power and balancing power markets [23]. In the regulating power market, the Transmission System Operator (TSO) purchases the regulating power that is usually provided by conventional generators. Moreover, both the production and consumption side, can submit the bids for the regulating power [23, 26]. The second, balancing power market, is used to settle the imbalances. The TSO purchases the balancing power to compensate for the imbalances caused by the market players. The production imbalance settlements are handled by a two-price balancing scheme, while the settlement of consumption imbalance is based on a one-price settlement scheme [23]. In the two-price balancing scheme, the deviations that contribute to the stability of the system, are traded at the DA market price. Meaning, the producer receives the DA price for excess production and producer pays the DA price in case of lack of production. On the contrary, the deviations that increase the imbalance of the system are penalized and traded according to regulation power prices. Meaning, the excess production receives a downward regulating power price lower than the DA price, and the lack of production pays the upward regulating power price higher than the DA price [26]. In a one-price balancing scheme, the consumer deviations pay the DA market price if system imbalance increases, and receive the balancing price if consumers contribute to the system balance. Hence, the prices for production imbalances are higher compared to consumption imbalances. To validate the effectiveness of the MPC based RT scheduling, simplified traditional RT scheduling in [27] is used for comparison and referred to as traditional RT scheduling. The total cost of the traditional RT scheduling is calculated which takes into account the penalty for the deviation from the DA pre-scheduled values based on a two-price settlement scheme [13].

As mentioned, due to deviation between DA and RT operation, forecasts must be updated and scheduling is performed in RT. Therefore, the MPC strategy is applied to the IES model as a prediction horizon scheme. The main principle of the MPC strategy is illustrated in the next subsection.

2.2 MPC strategy in RT scheduling

The schematic overview of the MPC based RT scheduling for the IES is illustrated in Fig. 1. Four aspects are discussed for MPC based RT optimization of the IES. The first aspect is the implementation process. The main principle of the MPC strategy is based on a closed loop with four modules, including system state measurement, updating of the forecast information, optimization over the prediction horizon, and execution of first control measures as it can be observed in the central part of Fig. 1. The four modules interact with each other and are implemented sequentially. The process of the closed loop is repeated with the time step forward. The MPC controller determines the optimal control actions in a prediction horizon and only the first control action of the prediction horizon is executed [28]. The measured and predicted values of the system are constantly updated as the time step moves forward. Once new predicted values are provided, MPC moves to the next time step and repeats the procedure. With such a principle, the deviation of RT scheduling caused by the prediction errors can be minimized by the MPC controller [13].

The second aspect of the MPC strategy is its application in the RT market. The RT market acts as the last opportunity to balance the prediction errors [24]. MPC strategy applied to the RT market replaces the original single-period optimization with a multi-period optimization. The time horizon of the optimization, i.e., the prediction horizon, needs to be selected. This aspect is shown in the central and lower part in Fig. 1. As can be seen, the objective of RT scheduling of the IES is to minimize the sum of the RT energy cost and regulation cost, while satisfying constraints of each energy sector and their coupling constraints. A detailed framework for the application of MPC strategy in RT scheduling will be designed.

The third aspect is the application of MPC in the IES. To achieve the RT optimal operation of the IES in the entire scheduling horizon and balance the multiple uncertainty sources of the IES in a more efficient manner, the MPC strategy is applied to the RT scheduling of the IES, namely MPC based RT scheduling of the IES. As an addition, the proposed MPC approach is taking into account the DA scheduling as seen in the left part of Fig. 1. The purpose is to minimize the deviation of the conventional generators in the RT compared to DA schedule. Therefore, the total objective is penalizing any deviation from DA pre-scheduled values in order to decrease the overall cost in the balancing market. The penalty for the deviation represents the simplified two-price balancing scheme which is included in the MPC in order to achieve higher economic and energy efficiency. To improve the operational flexibility of the IES, the power-to-x technology, thermal energy storage (TES) and gas storage are considered in the RT scheduling as well.

Once the model of the IES is established and the objective is introduced, the final part of the MPC approach in this paper is a selection of the uncertain parameters and forecasting. This aspect highly correlates to the second aspect of the MPC principle. As illustrated in the upper part of Fig. 1, four uncertainty sources are taken into account in the RT scheduling of the IES, which include the wind power output, electricity demand, heat demand and gas demand. The uncertainties on the left side are forecasted values used in the DA scheduling. The uncertainties on the right hand side include the historical and measured values. This data is used in the OL method in order to create a prediction horizon and update forecasts in each time step. The OL method is utilized to provide the forecast values of these uncertainty sources due to its advantage in lower computational burden and higher forecasting accuracy.

The overall objective of the MPC strategy is efficiently scheduling of the IES in the RT while updating the measured values and predicting a few steps in the future based on the updated RT measured values. Efficiently implies economic efficiency and flexibility increase while taking measured state and future information of the uncertainties into account.

To summarize, the MPC method used in RT scheduling is a forward-looking method that can provide a higher cost and energy efficiency compared to traditional RT scheduling [13, 28]. The characteristics of MPC based RT scheduling compared to traditional RT scheduling are summarized as follows. Firstly, MPC explores the possibility of the energy storages to provide balancing energy and increases the flexibility of the IES by the P2G and energy storages. Secondly, it is implemented as a rolling horizon scheme and finds the optimal solution for the present state based on the future forecasts. Moreover, it deals with the uncertainties in a forward-looking way and performs optimization for a specified prediction horizon.

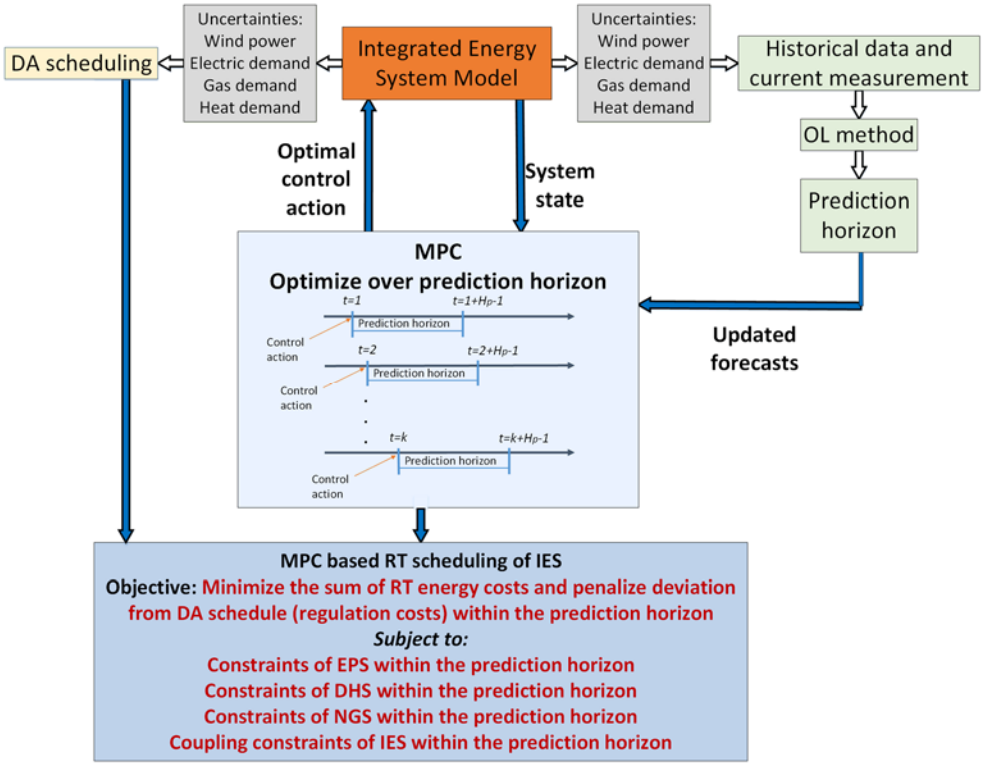

Fig. 1. Schematic overview of the MPC based RT scheduling for the IES

3. MPC based RT scheduling of IES

3.1 Mathematical formulation

The mathematical formulation for the MPC based RT scheduling of the IES is presented in this section. The MPC based RT scheduling aims to find an optimal solution based on the updated measured state and future predictions in the specified prediction horizon. The objective function in (1) consists of the operational cost of the CHP for power and heat production, gas source, TES operational costs, gas storage operational costs and the P2G operational cost to provide gas. Additionally, the wind spillage and load shedding costs are accounted for in the third part in (1). The penalty for deviating from the DA schedule values is presented in the last term in (1) to reduce the regulation of the conventional generators and to ensure that flexibility can be provided by the storages and P2G unit.

$$\begin{aligned} C_{total}(k) = \min \sum_{t=k}^{k+Hp-1} & \left\{ \sum_{j=1}^{n^{CHP}} C_j^{\mathrm{CHP,P}} P_{j,t}^{\mathrm{CHP,RT}} + \sum_{j=1}^{n^{CHP}} \left(C_j^{CHP,H} H_{j,t}^{\mathrm{CHP,RT}} \right) + \sum_{h=1}^{n^{HS}} \left(C_h^{\mathrm{HST,in}} H_{h,t}^{\mathrm{HS,in,RT}} + C_h^{\mathrm{HST,out}} H_{h,t}^{\mathrm{HS,out,RT}} \right) \right\} \\ + \sum_{t=k}^{k+Hp-1} & \left\{ \sum_{g=1}^{n^{GS}} C_g^{\mathrm{GS}} Q_{g,t}^{\mathrm{GS,RT}} + \sum_{s=1}^{n^{ST}} \left(C_s^{\mathrm{GST,in}} Q_{s,t}^{\mathrm{ST,in,RT}} + C_s^{\mathrm{GST,out}} Q_{s,t}^{\mathrm{ST,out,RT}} \right) + \sum_{p=1}^{n^{P2G}} C_p^{P2G} Q_{p,t}^{P2G,RT} \right\} \\ + \sum_{t=k}^{k+Hp-1} & \left\{ \sum_{e=1}^{n^{ED}} C_e^{VOLL} D_{e,t}^{\mathrm{ED,shed}} + \sum_{f=1}^{n^{ED}} C_f^{spill} W_{f,t}^{spill} \right\} \\ + \sum_{t=k}^{k+Hp-1} & \left\{ C_j^{penalty} \left| P_{j,t}^{\mathrm{CHP,RT}} - P_{j,t}^{\mathrm{CHP,DA}} \right| + C_j^{penalty} \left| H_{j,t}^{\mathrm{CHP,RT}} - H_{j,t}^{\mathrm{CHP,DA}} \right| + C_g^{penalty} \left| Q_{g,t}^{\mathrm{GS,RT}} - Q_{g,t}^{\mathrm{GS,DA}} \right| \right\} \end{aligned} \tag{1}$$

K is the total number of time steps in the scheduling horizon, k represents the current time step of the scheduling horizon, t is the index for time step in a prediction horizon and $k + H_p - 1$ is the length of a prediction horizon. The optimization problem is solved for each time step k. In each time step, all constraints in the prediction horizon should

be considered. That can be noted as $\forall t \in [k, k+H_p-1], \forall k \in K$. The notation is omitted from constraints below for the reasons of space. However, it must be accounted for.

The EPS constraints are summarized in (2)-(9). (2) represents the power balance constraint. (3) limits the maximum and minimum outputs of the CHP unit. (4) represents the transmission line capacity. (5) and (6) represent the downward and upward ramping rate limit, respectively. (7) gives the reference angle. (8) and (9) limit the wind spillage and load shedding by the measured values.

$$\sum_{j\in\Omega_n^{\mathrm{CHP}}} P_{j,t}^{\mathrm{CHP,RT}} + \sum_{f\in\Omega_n^{\mathrm{WT}}} \left(W_{f,t}^{RT} - W_{f,t}^{spill}\right) - \sum_{e\in\Omega_n^{\mathrm{ED}}} D_{e,t}^{\mathrm{ED,RT}} + \sum_{e\in\Omega_n^{\mathrm{ED}}} D_{e,t}^{\mathrm{ED,shed}} - \sum_{p\in\Omega_n^{\mathrm{P2G}}} D_{p,t}^{\mathrm{P2G,RT}} = \\ = \sum_{m\in\Lambda^{EPS}} B_{nm}\left(\delta_{n,t}^{RT} - \delta_{m,t}^{RT}\right), \ \forall n \in \Lambda^{\mathrm{EPS}} \tag{2}$$

$$P_j^{\mathrm{CHP,min}} \le P_{j,t}^{CHP,RT} \le P_j^{\mathrm{CHP,max}}, \ \forall j \in \Omega^{\mathrm{CHP}} \tag{3}$$

$$-P_{nm}^{\max} \le B_{nm}\left(\delta_{n,t}^{RT} - \delta_{m,t}^{RT}\right) \le P_{nm}^{\max}, \ \forall n,m \in \Lambda^{\mathrm{EPS}} \tag{4}$$

$$P_{j,t-1}^{\mathrm{CHP,RT}} - P_{j,t}^{\mathrm{CHP,RT}} \le RLD_j^{\mathrm{CHP}}, \ \forall j \in \Omega^{\mathrm{CHP}} \tag{5}$$

$$P_{j,t}^{\mathrm{CHP,RT}} - P_{j,t-1}^{\mathrm{CHP,RT}} \le RLU_j^{\mathrm{CHP}}, \ \forall j \in \Omega^{\mathrm{CHP}} \tag{6}$$

$$\delta^{RT}{}_{\mathrm{REF},t} = 0 \tag{7}$$

$$0 \le W_{f,t}^{spill} \le W_{f,t}^{RT}, \ \forall f \in \Omega^{\mathrm{WF}} \tag{8}$$

$$0 \le D_{e,t}^{\mathrm{ED,shed}} \le D_{e,t}^{\mathrm{ED}}, \ \forall e \in \Omega^{ED} \tag{9}$$

The DHS constraints are given in (10)-(23). (10) is the hydraulic constraint used to ensure that the mass flow going into a node equals to the one leaving the node. (11) represents the nodal heat balance constraint. (12) represents the temperature drop constraint in a pipeline, while (13) represents the temperature mix constraint. (14) limits heat power production from the CHP. (15) represents the permissible range of mass flow rate. (16) limits the maximum and minimum temperature of the water in the pipeline. (17) represent the TES state. (18) and (19) limit the TES discharge and charge rate, respectively. (20) represents the maximum and minimum TES capacity. (21)-(23) ensure only one process is available at the moment, either providing heat energy to the network or storing heat energy.

$$\sum_{m\in\Lambda_n} m_{mn,t}^{RT} = 0, \ \forall m \in \Lambda^{\mathrm{DHS}} \tag{10}$$

$$\sum_{j\in\Omega_n^{\mathrm{CHP}}} H_{j,t}^{\mathrm{CHP,RT}} + \sum_{h\in\Omega_n^{\mathrm{HS}}} \left(H_{h,t}^{\mathrm{HS,in,RT}} - H_{h,t}^{\mathrm{HS,out,RT}}\right) - \sum_{l\in\Omega_n^{\mathrm{HL}}} H_{l,t}^{\mathrm{HL}} = \\ = c \cdot m_{mn,t}^{RT} \cdot \left(\tau_{mn,t}^{in,RT} - \tau_{mn,t}^{out,RT}\right), \ \forall m \in \Lambda^{\mathrm{DHS}} \tag{11}$$

$$\tau_{mn,t}^{in,RT} - \tau^{\mathrm{a}} = e^{\frac{-\lambda_{mn,t}L_{mn}}{cm_{mn,t,0}^{RT}}}\left(\tau_{mn,t}^{out,RT} - \tau^{\mathrm{a}}\right), \ \forall m,n \in \Lambda^{\mathrm{DHS}} \tag{12}$$

$$\tau_{mn,t}^{out,RT} \sum_{m\in\Lambda_n} m_{mn,t}^{RT} = \sum_{m\in\Lambda_n}\left(m_{nm,t}^{RT} \cdot \tau_{nm,t}^{in,RT}\right), \ \forall m \in \Lambda^{\mathrm{DHS}} \tag{13}$$

$$H_j^{\mathrm{CHP,min}} \le H_{j,t}^{\mathrm{CHP,RT}} \le H_j^{\mathrm{CHP,max}}, \ \forall j \in \Omega^{\mathrm{CHP}} \tag{14}$$

$$m_{mn}^{\min} \le m_{mn,t}^{RT} \le m_{mn,t}^{\max}, \ \forall m,n \in \Lambda^{\mathrm{DHS}} \tag{15}$$

$$\tau_{mn}^{\mathrm{in/out,min}} \le \tau_{mn,t}^{\mathrm{in/out,RT}} \le \tau_{mn}^{\mathrm{in/out,max}}, \ \forall m,n \in \Lambda^{\mathrm{DHS}} \tag{16}$$

$$HS_{h,t+1}^{RT} = HS_{h,t}^{RT} + \left(H_{h,t}^{\mathrm{HS,out,RT}} - H_{h,t}^{\mathrm{HS,in,RT}}\right), \ \forall h \in \Omega^{\mathrm{HS}} \tag{17}$$

$$H_h^{\mathrm{HS,in,min}} x_{h,t}^{\mathrm{HS,in,RT}} \le H_{h,t}^{\mathrm{HS,in,RT}} \le H_h^{\mathrm{HS,in,max}} x_{h,t}^{\mathrm{HS,in,RT}}, \ \forall h \in \Omega^{\mathrm{HS}} \tag{18}$$

$$H_h^{\mathrm{HS,out,min}} x_{h,t}^{\mathrm{HS,out,RT}} \le H_{h,t}^{\mathrm{HS,out,RT}} \le H_h^{\mathrm{HS,out,max}} x_{h,t}^{\mathrm{HS,out,RT}}, \ \forall h \in \Omega^{\mathrm{HS}} \tag{19}$$

$$HS_h^{\min} \le HS_{h,t}^{RT} \le HS_h^{\max}, \ \forall h \in \Omega^{\mathrm{HS}} \tag{20}$$

$$x_{h,t}^{\mathrm{HS,out,RT}} + x_{h,t}^{\mathrm{HS,in,RT}} \le 1, \ \forall h \in \Omega^{\mathrm{HS}} \tag{21}$$

$$x_{h,t}^{\mathrm{HS,out,RT}} \in \{0,1\}, \ \forall h \in \Omega^{\mathrm{HS}} \tag{22}$$

$$x_{h,t}^{\mathrm{HS,in,RT}} \in \{0,1\}, \ \forall h \in \Omega^{\mathrm{HS}} \tag{23}$$

The NGS constraints include (24)-(38). (24) reflects the relationship between the pressure loss, pipeline parameters and gas flow. (25) is the nodal gas balance constraint, where the gas consumption by CHP is taken into account. Aside from the CHP, the NGS consists of a gas source, gas load, gas compressor, P2G and gas storage. (26)-(27) represents the constraint of GC to control the flow. (28)-(31) limit the operational range of the gas consumption of the gas source, gas production of the P2G, pressure in the pipeline and amount of gas flow in the pipeline, respectively. (32) represents the gas storage state. (33) and (34) limit the gas storage and gas discharge rates, respectively. (35)-(37) ensure only the gas charge or discharge is available at a time. (38) limits the maximum and minimum gas storage state.

$$\left(p_{n,t}^{RT}\right)^2-\left(p_{m,t}^{RT}\right)^2=Z_{nm}\left(S_{nm,t}^{RT}\right)^2,\ \ \forall n,m\in\Lambda^{\mathrm{NGS}} \tag{24}$$

$$\sum_{g\in\Omega_n^{\mathrm{GS}}}Q_{g,t}^{\mathrm{GS,RT}}+\sum_{s\in\Omega_n^{\mathrm{ST}}}\left(Q_{s,t}^{\mathrm{ST,out,RT}}-Q_{s,t}^{\mathrm{ST,in,RT}}\right)+\sum_{p\in\Omega_n^{\mathrm{P2G}}}Q_{p,t}^{\mathrm{P2G,DA}}$$
$$-\sum_{d\in\Omega_n^{\mathrm{GD}}}D_{d,t}^{\mathrm{GD}}-\sum_{g\in\Omega_n^{\mathrm{GC}}}D_{g,t}^{\mathrm{GC,RT}}-\sum_{j\in\Omega_n^{\mathrm{CHP}}}D_{j,t}^{\mathrm{CHP,RT}}=\sum_{m\in\Lambda_n}S_{nm,t}^{RT},\ \ \forall n,m\in\Lambda^{\mathrm{NGS}} \tag{25}$$

$$D_{g,t}^{\mathrm{GC,RT}}=\lambda_g^{\mathrm{GC}}S_{g,t}^{\mathrm{GC,RT}}=$$
$$=K^{\mathrm{GC}}Z_{\mathrm{a}}\left[\frac{T_s}{E^{\mathrm{GC}}\eta^{\mathrm{GC}}}\right]\left[\frac{c_k}{c_k-1}\right]\left[\left(CR\right)^{\frac{c_k-1}{c_k}}-1\right]S_{g,t}^{\mathrm{GC,RT}},\ \ \forall g\in\Omega^{\mathrm{GC}} \tag{26}$$

$$\left(p_{m,t}^{RT}\right)^2\le CR^2\left(p_{n,t}^{RT}\right)^2,\ \ \forall n,m\in\Lambda^{\mathrm{NGS}} \tag{27}$$

$$Q_g^{\mathrm{GS,min}}\le Q_{g,t}^{\mathrm{GS,RT}}\le Q_g^{\mathrm{GS,max}},\ \ \forall g\in\Omega^{\mathrm{GS}} \tag{28}$$

$$Q_p^{\mathrm{P2G,min}}\le Q_{p,t}^{\mathrm{P2G,RT}}\le Q_p^{\mathrm{P2G,max}},\ \ \forall p\in\Omega^{\mathrm{P2G}} \tag{29}$$

$$(p_{n,t}^2)^{\min}\le\left(p_{n,t}^{RT}\right)^2\le(p_{n,t}^2)^{\max},\ \ \forall n\in\Lambda^{\mathrm{NGS}} \tag{30}$$

$$-S_{nm}^{\max}\le S_{nm,t}^{RT}\le S_{nm}^{\max},\ \ \forall m,n\in\Lambda^{\mathrm{NGS}} \tag{31}$$

$$ST_{s,t+1}^{RT}=ST_{s,t}^{RT}+\left(Q_{s,t}^{\mathrm{ST,in,RT}}-Q_{s,t}^{\mathrm{ST,out,RT}}\right),\ \ \forall s\in\Omega^{\mathrm{ST}} \tag{32}$$

$$0\le Q_{s,t}^{\mathrm{ST,in,RT}}\le Q_s^{\mathrm{ST,in,max}}x_{s,t}^{\mathrm{ST,in,RT}},\ \ \forall s\in\Omega^{\mathrm{ST}} \tag{33}$$

$$0\le Q_{s,t}^{\mathrm{ST,out,RT}}\le Q_s^{\mathrm{ST,out,max}}x_{s,t}^{\mathrm{ST,out,RT}},\ \ \forall s\in\Omega^{\mathrm{ST}} \tag{34}$$

$$x_{s,t}^{\mathrm{ST,in,RT}}+x_{s,t}^{\mathrm{ST,out,RT}}\le 1,\ \ \forall s\in\Omega^{\mathrm{ST}} \tag{35}$$

$$x_{s,t}^{\mathrm{ST,in,RT}}\in\{0,1\},\ \ \forall s\in\Omega^{\mathrm{ST}} \tag{36}$$

$$x_{s,t}^{\mathrm{ST,out,RT}}\in\{0,1\},\ \ \forall s\in\Omega^{\mathrm{ST}} \tag{37}$$

$$ST_s^{\min}\le ST_{s,t}^{RT}\le ST_s^{\max},\ \ \forall s\in\Omega^{\mathrm{ST}} \tag{38}$$

The coupling components between different energy sectors are accounted for in (39)-(41). (39) represents the relationship between gas consumption and electricity generation for CHP units. (40) represents the relationship between the gas consumption and heat production for CHP units. (41) illustrates the relationship between power consumption and gas production for the P2G unit.

$$P_{j,t}^{\mathrm{CHP,RT}}=D_{j,t}^{\mathrm{CHP,RT}}\eta_j^{\mathrm{e}},\ \ \forall j\in\Omega^{\mathrm{CHP}} \tag{39}$$

$$H_{j,t}^{\mathrm{CHP,RT}}=D_{j,t}^{\mathrm{CHP,RT}}\eta_j^{h},\ \ \forall j\in\Omega^{\mathrm{CHP}} \tag{40}$$

$$Q_{p,t}^{\mathrm{P2G,RT}}=\eta_p^{\mathrm{P2G}}D_{p,t}^{\mathrm{P2G,RT}},\ \ \forall p\in\Omega^{\mathrm{P2G}} \tag{41}$$

To make the optimization problem computationally tractable, the equivalent or approximate transformations are necessary to cope with the nonlinear terms in the optimization. The absolute operator in (1) is linearized by replacing the absolute term with an auxiliary variable. Moreover, for each absolute term, two new constraints are introduced limiting the absolute term by the auxiliary variable. The bilinear terms of temperature and mass flow rate in (11)-(13) are linearized using Taylor. The gas flow equation in (24) is linearized by a piecewise linearization procedure [29]. After the transformation, the optimization problem is reformulated as a MILP. Lastly, the model is converted in p.u. system to decrease the computational burden [6, 29].

Additional constraints relate to the ramping rates in (5) and (6), which involve the previous state. These two constraints ensure that for every time step inside the prediction horizon, the ramping of the CHP does not exceed the maximum ramp rate limit. However, the ramping of CHP in the time steps of the scheduling horizon is not under any constraint. Hence, an additional constraint is provided to guarantee the feasibility of ramping limits throughout the scheduling horizon. With such a measure, a feasible optimization problem for the entire K is obtained in the prediction and scheduling horizon. Furthermore, similar constraints are applied to (17) and (32). As the storage state changes in the prediction horizon, the last value of the prediction horizon does not correspond to the actual value of the storage state. The reason behind this is that only the first control action from the prediction horizon is implemented. Therefore, additional constraints are applied and the storage states are feasible for the entire scheduling horizon.

As mentioned earlier, the IES contains four uncertainty sources, i.e. the wind power output, electricity demand, heat power demand, and gas demand. In order to provide updated forecasts for MPC, the forecasting method is applied. The OL method is utilized in the following section to provide the forecast values of these uncertainty sources.

3.2 Principle and application of OL method

In this subsection, the OL method is used to predict the future information of multiple uncertainty sources in the MPC based RT scheduling, including the wind power output, electricity demand, heat load, and gas demand [25, 30].

The linear regression method (LRM) is introduced as a basis of the OL method. The LRM forecasts future information by creating the relationship between the response and explanatory variables, e.g. wind power and wind speed respectively, for any given time. The relationship between wind speed and wind power for each time instant can be modelled through the least square (LS) estimation. However, three concerns should be taken into account for the LRM. Firstly, wind speed is forecasted in order to further obtain future forecasted wind power values. By using forecasting values to predict the future, the forecasting error is increased. Secondly, uncertain parameters can vary with time, e.g., seasonal effects of wind power. Seasonal effects can be taken into account through the estimation of model parameters on the sliding window. In other words, the LS can be performed for specified window size. For each time step, the regression parameters are recalculated leading to the third concern, i.e., the increased computational burden.

Two linear regression models can be differentiated. The first model considers simple mapping of the explanatory variable to response variable such as the mapping of wind speed to wind power as explained above. The second model is the autoregressive model, i.e. OL method, which is based on recursivity, i.e. the new update is based on the relationship between the last and the new data point [30]. Since the OL method can cope better with the highlighted concerns such as computational burden and increased forecast errors, it is implemented in this study based on the research in [30].

The basic principle of the OL method is described as follows [30]. An autoregressive model of order p is shown in (42) and its compact formulation in (43). y_t is the response variable, $\boldsymbol{x}_t = [1\ y_{t-1} \dots y_{t-p}]^T$ is the explanatory variable, $\boldsymbol{\beta}_t = [\beta_{t,0}\ \ \beta_{t,1} \dots\ \beta_{t,p}]^T$ is the model parameter and ε is the noise accounting for the deviation between the observed measurement and modelled relationship. The recursivity of the autoregressive model is controlled by the order of the model. To estimate model parameters β_t of the autoregressive model, the regressive least square (RLS) method is applied and β_t is obtained in each time step. The thorough procedure and elaboration of the OL method applied in this work can be found in [30, 27].

$$y_t = \beta_{t,0} + \beta_{t,1} y_{t-1} + \beta_{t,2} y_{t-2} + \dots + \beta_{t,p} y_{t-p} + \varepsilon_t \quad , \forall t \tag{42}$$

$$y_t = \boldsymbol{\beta}_t^{\mathrm{T}} \mathbf{x}_t + \varepsilon_t \quad , \forall t \tag{43}$$

Fig. 2 summarizes the application of the OL method in the MPC based RT scheduling. Wind power is used as an example. Since the scheduling horizon is set as 24 hours and the time resolution is 15 min, there are 96 time steps in the learning process. The OL method can predict the wind power output of the next step, as shown in the third step of Fig. 2. However, it is important to note that 97 time steps are used in the historical data to predict one step ahead.

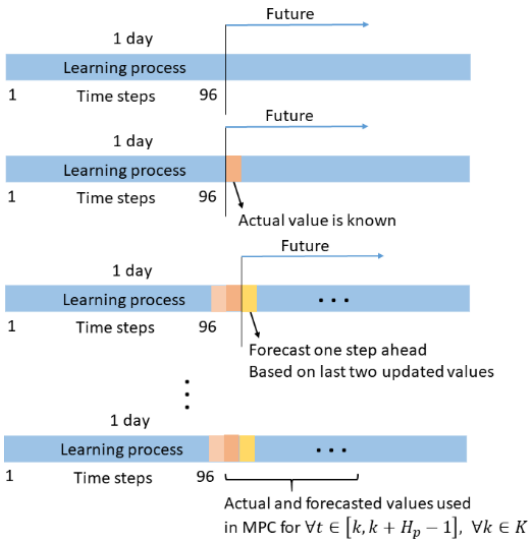

Fig. 2. Process of OL method in MPC based RT scheduling

Assume that a prediction horizon has H_p time steps in the MPC based RT scheduling. At the first time step of the prediction horizon, the measured values of the uncertainty sources are utilized, including the wind power output, electricity demand, gas demand and heat demand. At the second time step, the prediction values of each uncertainty source obtained by the OL method are utilized. For the rest H_p-2 time steps, the predicted values are generated based on forecast error distribution. It is assumed that the forecast errors of each uncertainty source follow the normal distribution with zero mean and a certain standard deviation. The standard deviation of each uncertainty source is calculated based on the average standard deviation of the previous day. Then the forecasted random errors sampled from the normal distribution are added to the predicted value obtained by the OL method. With the predicted values of uncertainty sources in the next few steps known, the operational cost over a prediction horizon is minimized.

3.3 Solution process

With the formulated model in subsection 3.1, the MPC controller calculates an optimal control measure sequentially for each step in the scheduling horizon. Once new measurements of the current step and predictions of the next few steps are obtained, a new optimization problem with updated states is solved. In a prediction horizon, only the control measure in the first time step is implemented. With such optimization approach, the total operational cost over the prediction horizon is minimized.

Fig. 3 summarizes the solution process of the MPC based RT scheduling for the IES. Firstly, the DA scheduling is performed for the entire day with a time resolution of one hour. Once the values of the DA scheduling are obtained, the MPC strategy can be applied. For each time step, the IES states are measured. Based on the current measurements, the OL method is utilized to predict the information of the next time step, and the forecasting error distribution is used for the rest of the forecasted values in the prediction horizon. Then the MPC based RT scheduling is performed to obtain a control measure for the current time step. Finally, the procedure is repeated until the maximum time step in the scheduling horizon is reached. Special attention is given to different time steps. Due to different time resolutions in DA and RT scheduling, the production cost of each unit, ramp rates and storage capacities must be adjusted according to the time resolution used.

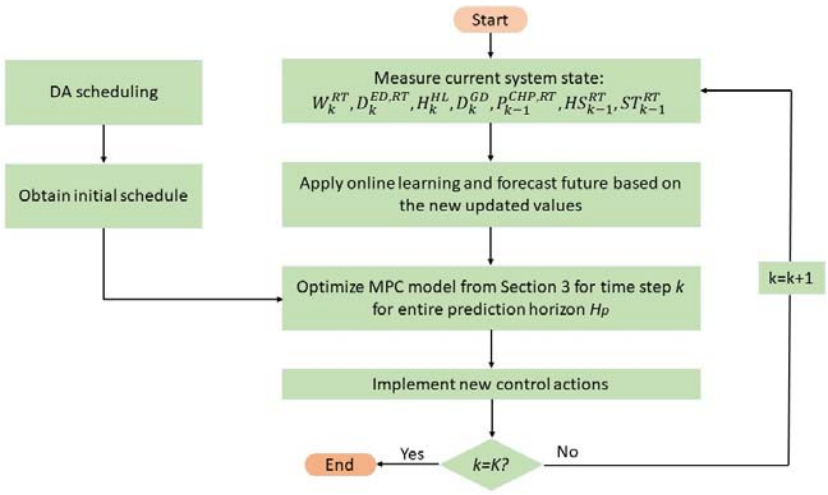

Fig. 3. Overview of the MPC based RT scheduling for the IES

4. Simulation results

Fig. A.1 in the Appendix shows the network of the test case system. [29] gives the operational costs for the DA schedule with a time resolution of one hour. The MPC based RT scheduling horizon is set to 24 hours with a time resolution of 15 minutes. To execute the RT scheduling every 15 minutes, the costs are converted into 15-minute intervals. The penalty for deviating from the pre-scheduled values is 150 $/MWh. The high cost is given to the penalty, as the balancing price is on average higher compared to DA price [26]. The measured and forecasted data for electricity demand and wind power can be found in the Transparency platform of the European Network of Transmission System Operators (ENTSO-E) and data from Germany (BZN|DE-LU) from January, 1st 2019 to January, 1st 2020 has been collected [31]. Data on natural gas and heat demand are collected from [6, 32]. The parameters of the NGS and DHS can be found in [6] and [10] respectively. In addition, the efficiency of useful heat production and efficiency of electricity generation provided from CHP are found in [33]. Depending on the time resolution used, parameters must be adjusted appropriately. The simulation is carried out and analyzed in MATLAB by using toolbox YALMIP and solver MOSEK [34, 35]. The parameters are summarized in Appendix and in [27].

The following subsections are introduced to validate the effectiveness of the MPC based RT scheduling method and analyze the selection of prediction horizon length. Section 4.1 validates the effectiveness of the OL method used in MPC. Section 4.2 studies the impact of prediction horizon length on computational efficiency. A longer prediction horizon can lead to a higher computational burden and bring larger forecast errors, while a shorter prediction horizon length cannot fully utilize the future information. Therefore, it is highly important to select a proper prediction horizon for the MPC. Section 4.3 verifies the advantages of MPC based RT scheduling over traditional RT scheduling. Section 4.4 analyses the operational cost and wind curtailment under different TES and gas storage capacities and prediction horizon lengths.

4.1 The benefit of using OL method in MPC

Selecting reasonable parameters for the forecasting model plays an important role in the OL method. The procedure for initialization of the parameters can be found in [30, 27]. The parameters β_0, β_1 and β_2 can be initialized at 0, 1.75 and -0.75, respectively based on the findings in [27]. The initialization for R_{t-1} is performed based on procedure given in [30, 27]. One day before the selected day is used to obtain the initial parameters, i.e. the final value of learning process time, equals 96 time steps for the wind power output.

The parameters of each uncertainty source differ, as shown in Table 1. The electricity demand and wind power data have a time resolution of 15 minutes. The standard deviation is calculated for a forecasting error which is a difference between measured and forecasted data for a day before the delivery day. It is used later on to obtain random numbers

based on the normal distribution for the current scheduling day. Due to the high variability of wind power, the standard deviation of forecast error of wind power is higher than that of the electricity demand. In contrast, the time resolution of the gas and heat demand data is one hour. Additionally, the measured gas and heat demands usually have a lower deviation from the forecasted values compared to the electric demand. Hence, the standard deviation equals half of the standard deviation of forecast error for electric demand. To conform with the time resolution of 15 minutes, the gas and heat demand data are extended to 96 time steps, with four equal values in each hour.

Table 1. Parameters for uncertainties used in OL method and predictions

Uncertainty	Learning process duration	Time resolution	β_0, β_1 and β_2			Prediction	Standard deviation
Wind power	1 day	15 min	0	1.75	-0.75	15 min ahead	0.0027
Electric demand	1 day	15 min	0	1.75	-0.75	15 min ahead	0.0012
Gas demand	2 days	1 hour	0	1.5	-0.5	1 h ahead	579.61e−6
Heat demand	2 days	1 hour	0	1.5	-0.5	1 h ahead	579.61e−6

In order to present the advantage of the OL method used in MPC, three cases are determined as described in Table 2. Case A represents the measured wind power and demand. Case B is based on the implementation of the OL method in MPC, while Case C is the conventional method based on a normal distribution with a known standard deviation of forecast errors. Standard deviations of forecast errors are taken from Table 1 and used to generate random numbers in Case C. The simulations were performed on a laptop with 2.7 GHz CPU and 16 GB RAM.

Table 2. Description of cases to create prediction horizon in MPC

Cases	Description of cases
Case A	Measured wind power and demand
Case B	Scheme with the prediction horizon based on OL method
Case C	Scheme with the prediction horizon based on the normal distribution with a known standard deviation of forecast errors

A comparison between three cases for electric demand and wind power is given in Fig. 4 a) and Fig. 4 b) respectively and the RMSE values of Cases B and C in comparison to the measured value in Case A are presented in Table 3. Case B follows the measured value in Case A and the predicted values are close to the measured values. The RMSE values between Cases A and B for electric demand and wind power are close to zero. Case B represents high accuracy predictions. On the contrary, Case C has high deviations from Case A as seen in Fig. 4. The RMSE values between Cases A and C are higher compared to Case B. Larger deviation is seen in Fig. 4 b) due to a higher forecast error of wind power. A larger RMSE value is observed in Case C for wind power compared to Case C for electric demand. Hence, the OL method provides accurate future predictions of wind power and electric demand. To conclude, the OL method is a highly accurate prediction method compared to the conventional method.

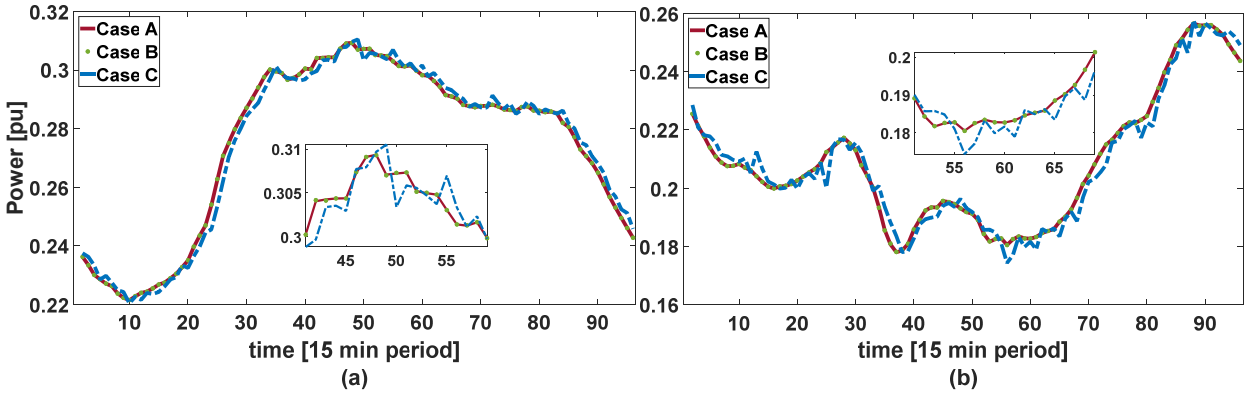

Fig. 4. Comparison of different schemes to create prediction horizon in MPC for a) electric demand b) wind power

Table 3. RMSE values for Case B and Case C

Cases	RMSE of wind power (pu)	RMSE of electric demand (pu)
Case B	0.706e−4	0.630e−4
Case C	0.0038	0.0028

4.2 Impact of prediction horizon on computational efficiency

The RT scheduling must be able to obtain the optimal control action within a reasonable time. The computational burden of MPC based RT scheduling depends mainly on the length of the prediction horizon. Therefore, it is very important to select a reasonable prediction horizon based on the required calculation time and storage capacities in the system.

Fig. 5 shows the changes of the calculation time as the length of the prediction horizon increases. It only considers the optimization in one time step, while the optimization has a different prediction horizon length. The prediction horizon ranges from five to 16 time steps. The prediction horizon with five time steps can account for the first hour of prediction. The first and second steps in a prediction horizon correspond to the measured values and predicted values, respectively. The last three values are based on the normal distribution with a known standard deviation of forecast errors. In the case of the prediction horizon length exceeding 16 time steps, the forecast error based on the normal distribution will increase over time. Higher forecast errors are not beneficial and valuable for the RT scheduling and, hence, prediction horizon length longer than 16 time steps is not explored.

A longer prediction horizon holds a higher amount of future information which is reflected in all the steps of the prediction horizon. Therefore, a longer prediction horizon can take action at the first step which might not be a case with the shorter prediction horizon due to the unavailability of future information. It can be seen from Fig. 5 that the calculation time of the RT scheduling with a prediction horizon of 16 time steps is far less than 15 minutes. Hence, the MPC based RT scheduling is feasible in terms of the calculation time, and the MPC method can be applied to RT operation.

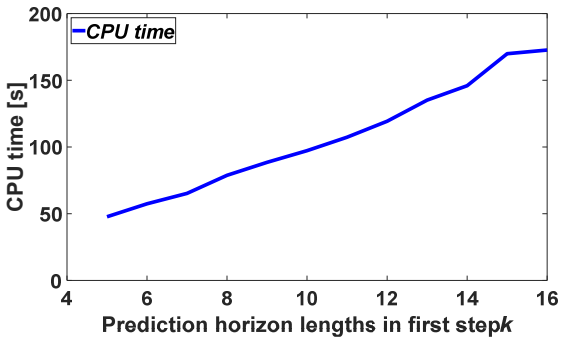

Fig. 5. Computational efficiency under different prediction horizon lengths

In summary, the length of the prediction horizon should be properly selected to ensure the application of the MPC method in RT scheduling. The selection should be based on the computational efficiency and forecast error, both of which increase with the length of the prediction horizon.

4.3 Validation of MPC strategy

Four cases are set to verify the effectiveness of the MPC based RT scheduling, as described in Table 4. Cases 1 and 2 are based on the MPC method with a time resolution of 15 minutes. The prediction horizon lengths are 8 and 16 time steps, respectively. Cases 3 and 4 represent RT scheduling performed in a traditional manner after the DA scheduling is performed. These two cases have different time resolutions.

Table 4. Description of cases

Cases	Description of cases

Case 1	MPC based RT scheduling with the length of prediction horizon $\mathbf{H_p=8}$
Case 2	MPC based RT scheduling with the length of prediction horizon $\mathbf{H_p=16}$
Case 3	Traditional RT scheduling in contrast to DA schedule with the time resolution of 1 hour
Case 4	Traditional RT scheduling in contrast to DA schedule with the time resolution of 15 minutes

Table 5 summarizes the total operating system cost of MPC based RT scheduling and traditional RT scheduling. The total operational system cost for MPC based RT scheduling is provided to full extend in Section 3.1 in (1). In the objective function (1), the deviations from the pre-scheduled values obtained in the DA scheduling are penalized in the current time step. On the contrary, the total operating system cost for traditional RT scheduling is based on the explanation in Subsection 2.1 and [27]. To elaborate, in the traditional RT scheduling, the penalty for deviation from DA pre-scheduled values is calculated after the RT dispatch and included in the total operating system cost in the RT. The results are presented for one day. The system costs of rescheduling in the RT in Cases 3 and 4 are lower compared to Cases 1 and 2. However, in the RT, Cases 3 and 4 redispatch on the basis of DA scheduling, resulting in an additional penalty cost. The system cost in the RT in column five is a result of joining the penalty cost to the system cost. By considering the penalty for deviation from DA scheduled values, the total operating system costs increase in Cases 3 and 4. Every deviation from the pre-scheduled DA values is penalized after traditional RT scheduling is adjusted. That is leading to higher total operating system costs in the RT of Cases 3 and 4 compared to Cases 1 and 2.

Further on, Case 1 reduces the cost by 2,1% and 2,13% compared to Cases 3 and 4, respectively. Case 2 reduces the cost by 0,45% and 0,47% compared to Cases 3 and 4, respectively. Due to higher marginal cost for the penalty for deviation from the pre-scheduled values in the DA than the marginal wind spillage cost, the total wind spillage cost as seen in column four is higher for Cases 1 and 2 compared to Cases 3 and 4. Moreover, the penalty in the objective function for traditional RT scheduling is neglected as mentioned earlier leading to lower wind spillage compared to MPC. Moreover, Case 2 has higher wind curtailment and total cost compared to Case 1. This is because a longer prediction horizon leads to a higher uncertainty level. Additionally, it can be noticed that RT scheduling with a time resolution of 1 h does not represent the real cost and state of the system. The time steps in between each hour in Case 3 are not taken into account resulting in differences in wind curtailment and cost in Cases 3 and 4. Moreover, in Case 3, the scheduling is not performed for every 15 minutes interval and the values are not being updated inside the hour.

Table 5. Comparison of system cost and wind spillage cost for four cases

Cases	**System cost ($)**	**Penalty ($)**	**Wind spillage cost ($)**	**Total system cost ($)**	**Cost loss compared to**	
					MPC: H_p=8	MPC: H_p=16
Case 1	736,95	-	121,90	736,95	-	-
Case 2	749,41	-	134,78	749,41	-	-
Case 3	360,95	391,83	96,29	752,78	2,10%	0,45%
Case 4	360,31	392,64	95,66	752,95	2,13%	0,47%

To summarize, MPC based approach includes the future predictions in the prediction horizon and finds the best solution for the present and future states of the system. In other words, the prediction horizon, as well as the future information, is not present in Case 4. The comparison between Cases 1 and 2 reveals that the higher prediction horizon in Case 2 has more information available on the future.

For further validation of MPC, the state of energy of the storages is examined. MPC cases, Case 1 and Case 2, are compared to Case 4 due to the equal time resolution for the RT scheduling. The comparison between Cases 1, 2 and 4 is shown in Fig. 6. The TES is providing the heat to the DHS in all three cases as shown in Fig. 6 a). The heat demand is decreasing towards the end of the day while the wind power is increasing as illustrated in Fig. 7. Therefore, in periods with high wind power, the CHP decreases its electricity production, and due to the linking of electricity and heat through the CHP unit, the heat provided by CHP decreases as well. Hence, the discharge rate of TES in moments of high wind power generation is increased. Such moments are seen at the end of the day, from around time step 70 to time step 90, in Fig. 7 and Fig. 6 a). The wind curtailment has a high increase at the end of the day and it occurs in the moments of excess generation, such as at the end of the day as shown in Fig. 6 b). Case 4 is following the elaborated explanation, and the lowest state of TES at the end of the day is seen in Case 4 compared to Case 1 and Case 2. The comparison reveals that the TES in Case 4 barely provides heat at each time step until the end of the scheduling

horizon when the TES starts discharging at a high rate. On the contrary, TES in Case 1 and Case 2 are gradually discharging throughout the day. The reason behind gradual discharging in Case 1 and Case 2 is that these cases are MPC based approaches and the next steps are accounted for in the prediction horizon. Moreover, both Case 1 and Case 2 are looking ahead and finding the best solution for the present and future states of the system. In other words, the prediction horizon, as well as the future information, is not present in Case 4 which results in high discharge by the end of the day. The comparison between Case 1 and Case 2 reveals that the higher prediction horizon in Case 2 has more information available on the future states. Therefore, a lower discharge rate of the TES in Case 2 is seen compared to Case 1. Besides, due to the longer prediction horizon in Case 2, it is possible to obtain future information regarding the high wind power. Hence, Case 2 increases the wind curtailment ahead of Case 1.

The gas storage states are presented in Fig. 6 c). As seen in Fig. 7, the gas demand is quite constant throughout the day compared to the rest of the uncertain parameters. Gas storage is not active in Case 4, while in Case 1 and Case 2, the gas storage is charging throughout the day. As already mentioned, traditional RT scheduling is not considering the penalty term in the objective function leading to the different rescheduling set points from the gas source. On the contrary, the MPC based RT scheduling would penalize the deviation if rescheduling is performed. Therefore, in order to have lower total system costs in RT, the gas is stored in the gas storage as seen in Case 1 and Case 2 instead of changing the setpoints of the gas source. Moreover, by taking the future information into account, Case 1 and Case 2 differ. Case 2 has a longer prediction horizon and it anticipates a very high wind in the future and allows a higher margin for the amount of the gas to be stored in the future. Furthermore, Fig. 6 d) shows the comparison of the gas provided by the P2G. The main function of the P2G unit is to convert the excess wind energy into natural gas. Case 4 represents the almost constant gas output from the P2G with a slight decrease in the moments of low wind power output. On the contrary, Case 1 and Case 2 anticipate future information regarding the wind power output, and as a result, these cases represent a more dynamic response of the P2G. In the moments of high wind power, wind spillage is high as seen in Fig. 6 b), and the P2G decreases the production of gas. The reason behind it is that the MPC based RT scheduling pursuits the optimal scheduling in the prediction horizon taking into account future states of the system, rather than the optimal scheduling in the current time step. In Case 1 and Case 2, the MPC method predicts the high wind curtailment at the end of the day and tries to schedule as economically as possible.

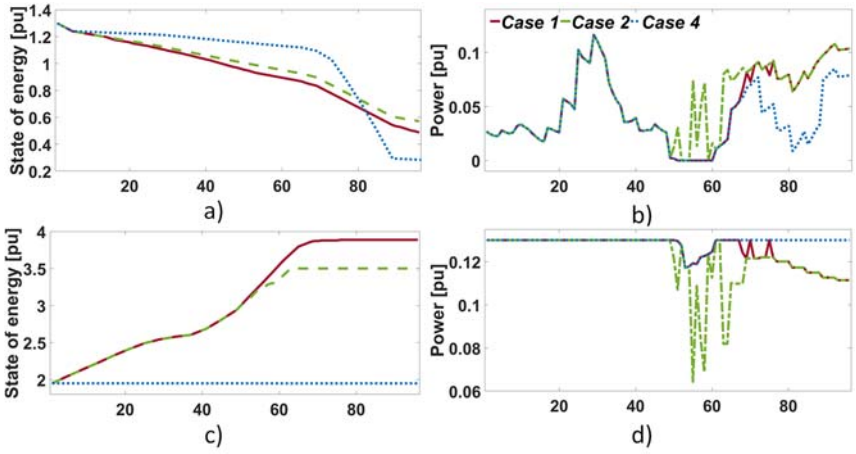

Fig. 6. Comparison between Case 1, Case 2 and Case 4 through entire scheduling horizon for a) heat storage state b) wind curtailment c) the gas storage state d) the P2G

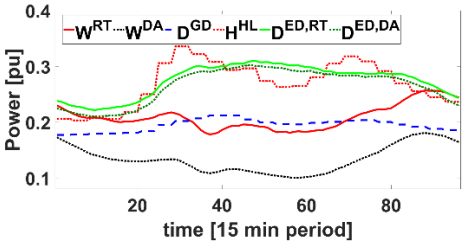

Fig. 7. Comparison of the actual and forecasted values of uncertainties considered in the IES

In summary, the MPC based RT scheduling takes into account the measured values and future forecast information. Compared with the traditional RT scheduling, it can schedule the generation and storages more optimally. In addition, the prediction horizon with eight time steps is appropriate for the current test system. However, the prediction horizon should take into account storage levels in the system as further discussed in Subsection 4.4.

4.4 Impact of storage capacity on prediction horizon

To investigate the impact of storage capacity on the prediction horizon length and consequently cost savings, the storage capacity and P2G capacity are increased by 54% in all the cases. Table 6 summarizes the total operating system cost for all the cases with increased storage levels and P2G capacity. The wind spillage cost is lower compared to Table 5 due to the additional P2G capacity. A significant increase in the total operating system costs is seen in Cases 3 and 4 compared to the initial cases in Table 5 due to additional penalty after the rescheduling has been performed. Further on, Case 1 can reduce the cost by 34,4% and 34,7% compared to Cases 3 and 4, respectively. Case 2 can reduce the cost by 33,8% and 34,1% compared to Cases 3 and 4, respectively. It is evident that by increasing the storage capacity and P2G capacity, the cost savings are higher by applying MPC based RT scheduling instead of traditional RT scheduling compared to Table 5.

Table 6. Comparison of system cost and wind spillage cost for four cases with a 54% increase of storages and P2G

Cases	System cost ($)	Penalty ($)	Wind spillage cost ($)	Total cost ($)	Cost loss compared to	
					MPC: H_p=8	MPC: H_p=16
Case 1	704.18	-	88.11	704.18	-	-
Case 2	710.71	-	94,89	710,71	-	-
Case 3	263.67	810.31	3.19	1073.98	34,4%	33,8%
Case 4	261.94	816.20	1.53	1078,14	34,7%	34,1%

The comparison between Cases 1 and 2 in both Table 5 and Table 6 reveal that the total operational RT system cost decreases with the increase of storage and P2G capacities. Total RT operational cost of Case 1 in Table 6 decreases by 4,5% compared to the cost of Case 1 in Table 5, while in Case 2 the cost in Table 6 decreases by 5,2% compared to the Case 2 in Table 5. Although Case 2 has a longer prediction horizon and brings higher cost and wind curtailment compared with Case 1, Case 2 can bring higher cost savings by considering larger storage capacity compared to Case 1. On the contrary, Case 4 in Table 6, results in negative cost savings compared to Case 4 in Table 5. The total cost in Case 4 in Table 6 increased by 30,2% compared to the total cost of Case 4 in Table 5.

As outlined above, the traditional RT scheduling does not provide any cost savings compared to MPC based RT scheduling despite the increased capacity of the storages and P2G unit. Moreover, by increasing the storage and P2G capacities, the traditional RT scheduling becomes economically inefficient and neglects the prominent flexibility that can be provided by the storages. In summary, in systems with higher storage levels, a longer prediction horizon can provide higher economic efficiency and reduce wind curtailment in the test system. Moreover, MPC based RT scheduling provides an economically efficient and flexible solution for the RT scheduling.

5. Conclusion and future work

This paper investigates MPC based real-time scheduling for the integrated energy system, which considers multiple uncertainty sources and utilizes the power-to-gas unit, thermal energy storage and gas storage devices to increase the flexibility. The online learning method is utilized to predict future information of the system in the decision making process. The length of the prediction horizon is selected according to the calculation burden, operational cost, wind power curtailment, and thermal energy storage and gas storage capacities. The main conclusions derived from the simulation results are as follows:

- Compared with the traditional real-time scheduling, the MPC based real-time scheduling can reduce the wind curtailment and improve the economic efficiency by accounting for the measured values and future prediction information of the integrated energy system.
- The online learning method combined with MPC can provide accurate predictions and avoid a high computational burden for the MPC based real-time scheduling.
- The MPC based real-time scheduling provides higher efficiency and flexibility to the system by introducing a higher prediction horizon taking into account larger part of future information. Moreover, systems with higher storage levels and a longer prediction horizon can provide higher economic efficiency and reduce wind curtailment.
- The length of prediction horizon and time resolution are of great importance for MPC based real-time scheduling of the integrated energy system. The length of the prediction horizon should be selected based on the required computational efficiency and storage capacity in the system. A longer prediction horizon shows higher total cost savings in the integrated energy system with larger storages.

A promising solution for the future would be further increasing the gas storage and power-to-gas unit to take advantage of the wind power. Moreover, the gas is virtually stored in the pipeline, namely the linepack, which can increase economic efficiency. A limitation of this work is that the gas linepack was not considered. Furthermore, the online learning method could be used for more than one step ahead predictions and more reliable predictions for the steps obtained after the online learning method could be considered. One should also take into account the load shedding in the real-time schedule that corresponds to the negative forecast errors of wind power.

Acknowledgments

The work was supported by the EUD Programme through the 'Coordinated Operation of Integrated Energy Systems (CORE)' project under the grant 64017-0005. We are grateful for the research provided by ELMA group at the DTU Center for Electric Power and Energy (CEE), Summer School 2019 "Data-Driven Analytics and Optimization for Energy Systems. We are also thankful to Mikhail Skalyga for providing insights into the online learning method.

Data availability

Datasets related to this article can be found at https://github.com/Ana-Turk/Electronic-companion-Datasets-parameters-and-methods hosted at GITHUB [27].

Appendix A

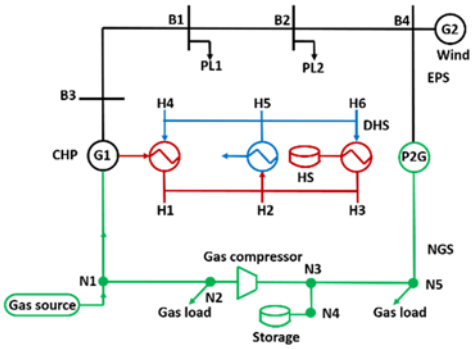

Fig. A.1. Test system

Table A.1. Parameter values (per quarter hour of period length)

Parameter	Value [p.u.]	Parameter	Value [p.u.]
$\lambda_{mn,t}$	0.189,0.236, 0.21,0.21[W/m°C]	$(p^2_{n,t})^{\min}$	0,25 [kPa^2]
η^{GC}	0,85	$(p^2_{n,t})^{\max}$	4 [kPa^2]
η^{e}_{j}	0,4	$(p^2_{n,t})^{reference}$	1 [kPa^2]
η^{h}_{j}	0,38	$P^{CHP,\min}_{j,t}$	0
η^{P2G}_{k}	0,75	$P^{CHP,\max}_{j,t}$	1
τ^{a}	10 [°C]	$P^{\max}_{nm}$	0,5 p.u.
$\tau^{in/out,\min}_{mn,t}$	30 [°C]	$Q^{GS,\min}_{g}$	0
$\tau^{in/out,\max}_{mn,t}$	80 [°C]	$Q^{GS,\max}_{g}$	7,7
c_p	4,64668e-6 p.u.h/kgK	$Q^{P2G,\min}_{k}$	0
c_k	1,3	$Q^{P2G,\max}_{k}$	0,13
CR	1,4	$Q^{ST,in/out,\min}_{s}$	0
E^{GC}	0,99	$Q^{ST,in/out,\max}_{s}$	0,13
$H^{CHP,\min}_{j}$	0	Reactance	0.1577 p.u.
$H^{CHP,\max}_{j}$	1	RLD^{CHP}_{j}	9 p.u./h
$H^{HS,in/out,\min}_{h}$	0	RLU^{CHP}_{j}	9 p.u./h
$H^{HS,in/out,\max}_{h}$	0,26	$S^{\max}_{nm}$	5
HS^{0}_{h}	1,3	P_{base}	1 MW
$HS^{\min}_{h}$	0,26	ST^{0}_{s}	1,95
$HS^{\max}_{h}$	2,34	$ST^{\min}_{s}$	0,26 [p.u.h]
K^{GC}	0,0854	$ST^{\max}_{s}$	3,9 [p.u.h]
$L_{mn}(L_{12}, L_{23}, L_{65}, L_{54})$	271.3,235.4, 177.3, 102.8 [m]	T_s	530 °R
$m^{\min}_{mn,t}$	1 [kg/s]	Z_a	0,95
$m^{\max}_{mn,t}$	3 [kg/s]	$Z_{nm}(Z_{12}, Z_{23}, Z_{34}, Z_{35})$	44.8085;59.7447; 29.8723;44.80 [kPa^2/(pu)^2]

References

[1] IRENA, “Wind energy,” 2019. [Online]. Available: https://www.irena.org/wind.

[2] European Commision, “Paris Agreement,” [Online]. Available: https://ec.europa.eu/clima/policies/international/negotiations/paris_en.

[3] Wind Denmark, “Current energy production,” 2020. [Online]. Available: https://en.winddenmark.dk/wind-in-denmark/current-energy-production.

[4] Energinet, “PTX IN DENMARK BEFORE 2030: Short term potential of PtX in Denmark from a system perspective,” April 2019. [Online]. Available: https://energinet.dk/-/media/8BF0CD597E1A457C8E9711B50EC2782A.PDF.

[5] Meibom P, Hilger K. B, Madsen H, Vinther D. “Energy Comes Together in Denmark: The Key to a Future Fossil-Free Danish Power System,” *IEEE Power and Energy Magazine,* 2013; 11(5): 46-55.

[6] Zeng Q, Fang J, Li J, Chen Z. “Steady-state analysis of the integrated natural gas and electric power system with bi-directional energy conversion,” *Applied Energy,* 2016; 184: 1483-1492.

[7] Correa-Posada C. M, Sánchez-Martín P. “Integrated Power and Natural Gas Model for Energy Adequacy in Short-Term Operation,” *IEEE Transactions on Power Systems,* 2015; 30(6): 3347-3355.

[8] Ordoudis C, Delikaraoglou S, Pinson P, Kazempour J. “Exploiting flexibility in coupled electricity and natural gas markets: A price-based approach,” in *IEEE Manchester PowerTech*, Manchester, 2017.

[9] Zeng Q, Zhang B, Fang J, Chen Z, “A bi-level programming for multistage co-expansion planning of the integrated gas and electricity system,” *Applied Energy,*2017; 200: 192-203.

[10] Liu X, Wua J, Jenkins N, Bagdanavicius A. “Combined analysis of electricity and heat networks,” *Applied Energy,*2016; 162:1238-1250.

[11] Zeng Q, Conejo A. J, Chen z, Fang J. “A Two-stage Stochastic Programming Approach for Operating Multi-energy Systems,” in *IEEE Conference on Energy Internet and Energy System Integration*, Beijing, 2017.

[12] Mazzi N, Pinson P. “Wind power in electricity markets and the value of forecasting,” *Renewable Energy Forecasting*, 2017; 259-279.

[13] Du Y, Pei W, Chen N, Ge X, Xiao H. “Real-time microgrid economic dispatch based on model predictive control strategy,” *Journal of Modern Power Systems and Clean Energy,* 2017; 5(5): 787–796.

[14] Michèle A, Andersson G. “Model Predictive Control of Energy Storage including Uncertain Forecasts,” 2011.

[15] Holjevac N, Capuder T, Kuzle I. “Adaptive control for evaluation of flexibility benefits in microgrid systems,” *Energy,* 2015; 92(3): 487–504.

[16] Holjevac N, Capuder T, Zhang N, Kuzle I, Kang C. “Corrective receding horizon scheduling of flexible distributed multi-energy microgrids,” *Applied Energy,* 2017; 207: 176–194.

[17] Li Z, Zang C, Zeng P, Yu H. “Combined two-stage stochastic programming and receding horizon control strategy for microgrid energy management considering uncertainty,” *Energies,* 2016; 9(7): 1-16.

[18] Rahmani-Andebili M, Fotuhi-Firuzabad M. “An Adaptive Approach for PEVs Charging Management and Reconfiguration of Electrical Distribution System Penetrated by Renewables,” *IEEE Transactions on Industrial Informatics,* 2018; 14(5): 2001-2010.

[19] Rahmani-Andebili M. “Dynamic and adaptive reconfiguration of electrical distribution system including renewables applying stochastic model predictive control,” *IET Generation, Transmission & Distribution,* 2017; 11(16): 3912-3921.

[20] Rahmani-Andebili M. “Chapter 9: Cooperative Distributed Energy Scheduling in Microgrids,” in *Electric Distribution Network Management and Control*, Singapore, Springer Singapore, 2018.

[21] Rahmani-Andebili M. “Scheduling Deferrable Appliances and Energy Resources of a Smart Home Applying Multi-Time Scale Stochastic Model Predictive Contro,” *Sustainable Cities and Society,* 2017; (32): 338-347.

[22] Rahmani-Andebili M. “Stochastic, adaptive, and dynamic control of energy storage systems integrated with renewable energy sources for power loss minimization,” *Renewable Energy,* 2017; 113: 1462-1471.

[23] Energinet, “Rules and Regulations in the Danish electricity market - Market regulations,” Dec 2017. [Online]. Available: https://en.energinet.dk/Electricity/Rules-and-Regulations/Market-Regulations.

[24] Wang Q, Zhang C, Ding Y , Xydis G, Wang J, Østergaard J. “Review of real-time electricity markets for integrating Distributed Energy Resources and Demand Response,” *Applied Energy,* 2015; 138: 695–706.

[25] Morales J. M, Conejo A. J, Madsen H, Pinson P, Zugno M. Integrating Renewables in Electricity Markets, New York: Springer, 2014.

[26] Energinet, Danish Energy Agency, “Nordic Power Market Design adn thermal Power Plant Flexibility,” 2018, May.

[27] “Turk A. "Electronic companion",2020.Available:https://github.com/Ana-Turk/Electronic-companion-Datasets-parameters-and-methods,” [Online].

[28] Velasquez M. A, Barreiro-Gomez J, Quijano N, Cadena A. I, Shahidehpour M. “Distributed model predictive control for economic dispatch of power systems with high penetration of renewable energy resources,” *International Journal of Electrical Power & Energy Systems,* 2019; 113: 607-617.

[29] Turk A, Wu Q, Zhang M, Østergaard J. “Day-ahead stochastic scheduling of integrated multi-energy system for flexibility synergy and uncertainty balancing,” *Energy,* 2020; 196:1-17.

[30] DTU CEE Summer school, “Data-Driven Analytics and Optimization for Energy Systems,” 2019. [Online]. Available: https://energy-markets-school.dk/summer-school-2019/.

[31] ENTSO-E, “Transparency platform,” ENTSO-E, 2020. [Online]. Available: https://transparency.entsoe.eu/dashboard/show.

[32] Affaldvarme Aarhus, “Varmeplanaarhus,” Affaldvarme Aarhus, 2020. [Online]. Available: https://www.varmeplanaarhus.dk/.

[33] European Comission, Eurostat, “Combined Heat and Power (CHP) Generation,” Eurostat, 2017 May.

[34] Yalmip, “Yalmip,” Oct 2020. [Online]. Available: https://yalmip.github.io/?n=Main.License.

[35] MOSEKApS, “The MOSEK optimization toolbox for MATLAB manual. Version 9.0,” 2019. [Online]. Available: http://docs.mosek.com/9.0/toolbox/index.html.